

## Effect of Cholesterol on the Properties of Phospholipid Membranes. 2. Free Energy Profile of Small Molecules

Pál Jedlovszky\*,†

Department of Colloid Chemistry, Eötvös Loránd University, Pázmány Péter sny. 1/a, H-1117 Budapest, Hungary

Mihaly Mezei‡

Department of Physiology and Biophysics, Mount Sinai School of Medicine of the New York University, New York, New York 10029

Received: August 22, 2002; In Final Form: December 12, 2002

The effect of cholesterol on the properties of lipid membranes has been investigated by computer simulations. For this purpose, the crossmembrane free energy profiles of eight penetrants, i.e.,  $\text{H}_2\text{O}$ ,  $\text{O}_2$ ,  $\text{CO}$ ,  $\text{CO}_2$ ,  $\text{NO}$ ,  $\text{NH}_3$ ,  $\text{CHCl}_3$ , and formamide, have been calculated by the cavity insertion Widom (CIW) method in four simulated dimyristoylphosphatidylcholine (DMPC)/cholesterol mixed membranes of different compositions, i.e., containing 0%, 4%, 8%, and 40% cholesterol. The compositions of the simulated two component membranes have been selected from both sides of the DMPC/cholesterol miscibility gap, and the pure DMPC membrane has been regarded as a reference system. It is found that cholesterol increases the amount of spherical cavities in the membrane region in which their OH group is located and, hence, lowers the solvation free energy of the penetrants in this region. For strongly polar solutes, this is the region of the minimum of the free energy profiles, and hence, by lowering this minimum, cholesterol increases the free energy barrier of the crossmembrane transport of such penetrants. On the other hand, for larger and apolar or moderately polar solutes, such as  $\text{CO}_2$  and  $\text{CHCl}_3$ , the free energy profiles exhibit a peak in this region. In the case of  $\text{CHCl}_3$ , cholesterol is found to lower and, above a certain concentration, eliminate this peak and thus considerably decrease the free energy barrier of the crossmembrane transport of this molecule. On the other hand, in the case of  $\text{CO}_2$ , this peak is transformed to a dip by cholesterol, and hence, the free energy barrier of the crossmembrane penetration of  $\text{CO}_2$  is first lowered by increasing the fraction of cholesterol in the membrane up to a certain concentration, above which a further increase of the amount of cholesterol results in an increasing free energy barrier. Finally, in the case of the diatomic penetrants, neither the maximum nor the minimum of the free energy profiles is located in the region where cholesterol lowers the solvation free energy, and thus, the free energy barrier of the crossmembrane transport of these molecules is not affected by cholesterol.

### Introduction

The transport of small particles (ions, molecules) across biological membranes is a key process of the metabolism of the cells. Various regulatory mechanisms are responsible for the transport of the majority of such particles. For instance, ions can only cross the cell membrane with the aid of special membrane-bound protein molecules.<sup>1</sup> On the other hand, some small, uncharged molecules of vital biological importance (e.g.,  $\text{H}_2\text{O}$ ,  $\text{O}_2$ ,  $\text{CO}_2$ ,  $\text{NO}$ ,  $\text{NH}_3$ , formamide, urea, etc.) can permeate the membrane in appreciable rate by simple diffusion, without the aid of any special transport mechanism facilitated by transport proteins.<sup>2–4</sup> The transport properties of these molecules across the membrane of living cells are extremely important in several physiological processes. For instance, the entire respiratory mechanism is based on the ability of the  $\text{O}_2$  and  $\text{CO}_2$  molecules to cross promptly the membrane of several types of human cells. The same ability of the  $\text{CO}$  molecule is required to make it a dangerous poison. The crossmembrane transport of various small molecules (e.g., water, ammonia, urea) is one of the basic processes of excretion. The  $\text{NO}$  molecule is an

important element of the blood pressure regulation mechanism. This function again requires the ability of  $\text{NO}$  to go through the cell membrane promptly.<sup>4</sup> The anesthetic behavior of molecules such as  $\text{CHCl}_3$  and  $\text{N}_2\text{O}$  is related to their crossmembrane transport properties, as well.

The cell membrane itself is a rather complex assembly of various molecules, such as lipids, segments of proteins of various types and functions (e.g., channel-forming and signal transduction proteins), dissolved smaller molecules, etc. Among the many constituents, phospholipid molecules, such as dimyristoylphosphatidylcholine (DMPC) and dipalmitoylphosphatidylcholine (DPPC), can be regarded as the main components that form the medium of the membrane. Besides the phospholipid molecules, cholesterol is one of the most frequent, ubiquitous membrane components. Its concentration in the membrane can be as high as 50% in some cases.<sup>5</sup>

Cholesterol and phospholipids are not perfectly miscible with each other.<sup>5–11</sup> For instance, at 37 °C DMPC and cholesterol are not miscible in the cholesterol mole fraction range of about 0.1–0.3.<sup>5</sup> This composition range roughly covers the cholesterol content of the membranes of living cells; hence, in the cell membranes domains of high and low cholesterol content should be separated.

\* E-mail: pali@para.chem.elte.hu.

† E-mail: mezei@inka.mssm.edu.

The presence of cholesterol influences, among many other properties, the transport of small molecules across phospholipid membranes. It is known experimentally that passive permeability of phospholipid bilayer membranes is reduced upon adding cholesterol to the system.<sup>12–15</sup> This observation is rather surprising, as it contradicts simple chemical intuition. The cholesterol molecule is considerably shorter than the most frequent membrane-constituent phospholipid molecules, such as DMPC and DPPC. Hence, when a lipid molecule is replaced by cholesterol in the membrane, one can expect that the density decreases and relatively large voids appear at specific positions along the membrane normal (e.g., in the region of the head-groups), whereas at other positions (e.g., along the hydrocarbon chains where the cholesterol molecules are located) no such changes appear. Such changes would imply easier diffusion of the penetrants at least through those regions in which the density is decreased, and thus an increased permeability of the membrane: exactly the opposite of what is found experimentally.

In order to understand the molecular level origin of the experimentally observed behavior and to clarify the seeming contradiction between the intuition and the experimental facts, computer simulation methods can provide an efficient tool. However, in performing such a simulation one has to face several difficulties. The direct simulation of the permeation of a molecule through a membrane formed by a bilayer of phospholipid molecules is virtually impossible, since the computational cost of such a calculation is several orders of magnitude beyond the computational capacity of the present day simulations. Diffusion of small penetrants across a fully hydrated lipid bilayer has, to our knowledge, only been studied in the pioneering works of Marrink and Berendsen.<sup>16,17</sup> In these works, a different method has been used for studying the crossmembrane transport of  $H_2O$ ,<sup>16</sup>  $O_2$ , and  $NH_3$ .<sup>17</sup> They determined the diffusion constant profile of these molecules by inserting test molecules in several positions along the membrane normal and probed their local diffusion constants at the test positions. However, this calculation can only provide approximate results since the entire crossmembrane profile is estimated by the few values obtained at the test positions, and it is still computationally rather demanding.

An alternative way of investigating crossmembrane transport processes is the calculation of the crossmembrane free energy profile (FEPR) of the penetrant molecules. Since the free energy gradient of the penetrant along the membrane normal represents the thermodynamic driving force of its crossmembrane transport, the determination of its free energy profile can provide important information on the physical background of the permeation process through the membrane. However, mapping the free energy in such strongly inhomogeneous systems as a lipid membrane, consisting of aqueous, ionic, and apolar regions, is still a rather difficult task. In fact, the calculation of the solvation free energy even in a homogeneous environment is computationally far more demanding than simply sampling configurations from an equilibrium ensemble, as done in usual computer simulations. In the case of lipid membranes, the situation is further complicated by the fact that even the exploration of the configurational space of the system is rather slow. It may result that the simulated sample configurations show variations of the local environment at different positions located at the same depth in the membrane. Therefore, several free energy calculation methods, based on sampling a small domain of the simulated system, that are well tested in a homogeneous environment, can

show in the membrane strong dependence of the results on the lateral position chosen for the calculation and, hence, be unreliable.<sup>18</sup>

Due to these difficulties, only a few transmembrane free energy profile simulation studies have been reported so far. Stouch et al. have determined the FEPR of apolar solutes from direct simulations.<sup>19,20</sup> However, their calculations have been limited to the hydrocarbon phase of the membrane. In their aforementioned study, Marrink and Berendsen have calculated the FEPR of  $H_2O$ ,  $NH_3$ , and  $O_2$  across a fully hydrated DPPC bilayer.<sup>16,17</sup> In the case of water, they have used different methods for determining the excess free energy in the aqueous, interfacial, and hydrocarbon regions of the membrane,<sup>16</sup> whereas the FEPR of  $NH_3$  and  $O_2$  have been determined<sup>17</sup> using the Widom test particle insertion method.<sup>21</sup> Recently, we have proposed a cavity insertion variant of the original Widom algorithm,<sup>22</sup> named as cavity insertion Widom (CIW) method, and have shown that this method can be used for a relatively fast determination of the FEPR of several solutes across a lipid membrane.<sup>22</sup> In a CIW calculation, similar to the particle creation step of the cavity biased grand canonical Monte Carlo simulations,<sup>23,24</sup> the test particle is only inserted into cavities of suitably large radius, and hence, the computationally demanding calculation of the large number of test positions contributing negligibly to the calculated ensemble averages can be avoided. The CIW method retains the advantage of the original Widom method in that positions throughout the entire system simulated are tested, and thus, the results are averaged over all lateral positions located at the same depth along the membrane normal. This can largely reduce the uncertainty of the results caused by the slow exploration of the configurational space in the simulation. Another advantage of the method is that the slowest steps of the calculation, i.e., the generation of the equilibrium sample configurations by computer simulation and the selection of the array of cavities for the test particle insertion, are independent from the type of test molecule used. Therefore, once the FEPR of a given solute molecule is determined, the procedure can easily be repeated for a set of different solutes for a relatively little extra computational cost. On the other hand, we have also shown that the CIW method has to be regarded as an approximate method, as the inaccuracy of the obtained results is in the range of about 0.2–2 kcal/mol for small, uncharged solutes, and it strongly depends on the type of solute molecule.<sup>22</sup> Therefore, the precision of the method has to be estimated for each solute molecule independently. Such estimation can be done by determining the solvation free energy of the solute molecules in water by different free energy calculation methods, including CIW. The obtained crossmembrane FEPRs have to be interpreted then considering also the obtained precision of the calculation.

In this paper, we report Monte Carlo simulations of DMPC/cholesterol mixed bilayers of four different compositions, and results of CIW calculations of the FEPR of eight penetrants, i.e.,  $H_2O$ ,  $O_2$ ,  $CO$ ,  $CO_2$ ,  $NO$ ,  $NH_3$ ,  $CHCl_3$ , and formamide, across these bilayers. One of the simulated bilayers is pure DMPC, acting as a reference system. Two of the simulated compositions have been chosen from the cholesterol-poor side and one from the cholesterol-rich side of the immiscibility region of DMPC and cholesterol. This selection of the systems allows us to analyze the effect of the presence and concentration of cholesterol on the permeability properties of phospholipid membranes for penetrants of various types at a molecular level detail.

**TABLE 1: Composition and Cell Size Parameters of the Four Systems Simulated**

system	cholesterol concentration (mol %)	prism height (Å)	hexagon edge (Å)
I	0	79.01	23.61
II	4	79.86	23.42
III	8	80.28	23.44
IV	40	80.83	22.63

## Methods

**Monte Carlo Simulation of the DMPC/Cholesterol Mixed Bilayers.** Fully hydrated mixed bilayers of DMPC and cholesterol of four different compositions have been simulated on the canonical ( $N, V, T$ ) ensemble at 310 K. The simulations have been performed by the program MMC.<sup>25</sup> DMPC and cholesterol molecules have been described by the all-atom CHARMM22 force field,<sup>26</sup> whereas for water, the TIP3P potential model<sup>27</sup> has been used. Thus, the electrostatic and nonelectrostatic part of the interatomic interactions have been described by a Coulombic and a Lennard-Jones term, respectively. Water–water and water–lipid interactions have been truncated to zero beyond the center–center distances of 12 and 16 Å, respectively. A similar combination has been found to behave close to the infinite cutoff system for a hydrated lipid monolayer.<sup>28</sup> The two layers of the membranes have been built up by 25–25 molecules, and the bilayers have been hydrated by 2033 water molecules. The number of cholesterol molecules in each side of the bilayer has been set to 0, 1, 2, and 10 in the four systems simulated. Thus, one of the systems (referred here as system I) has consisted of a bilayer of pure DMPC and is regarded as a reference system. Two systems (systems II and III) have been chosen from the cholesterol-poor side and one (i.e., system IV) from the cholesterol-rich side of the DMPC/cholesterol miscibility gap. A hexagonal prism shaped basic simulation box has been used in order to maximize the distance of two periodic images of a given particle in lateral directions. The edge of the basic hexagon and the height of the prism have been set by a preceding simulation, performed on the isothermal–isobaric ( $N, p, T$ ) ensemble. Starting configurations have also been taken from these simulations, the details of which have been described in detail in our previous paper.<sup>29</sup> The composition and cell size parameters of the systems simulated are summarized in Table 1. The four simulations have been performed in the same way as described in our previous paper,<sup>29</sup> apart from the obvious lack of volume changing steps here. Thus, water and lipid moves have been performed in an alternating order. In a water move, a water molecule has been randomly translated and rotated by no more than 0.3 Å and 20°, respectively. In 20% of the lipid moves, a DMPC or cholesterol molecule has been randomly translated and rotated around a randomly chosen space-fixed axis. In the rest of the lipid moves, a torsional angle has been randomly changed. Overall lipid rotations as well as torsional changes have been performed using the novel extension biased method.<sup>30</sup> The systems have been equilibrated in  $5 \times 10^7$  Monte Carlo steps long runs. In the production phase, 2000 sample configurations, separated by  $10^5$  Monte Carlo steps each, have been saved for the CIW calculations in each system.

**CIW Calculations. The CIW Method.** In Widom-type calculations,<sup>21</sup> the excess free energy of a solute molecule is obtained by inserting it at random positions into the equilibrated ( $N, V, T$ ) ensemble sample configurations of the system, and averaging the  $\exp(-U_{\text{test}}/k_{\text{B}}T)$  factor over all test positions, where  $U_{\text{test}}$  is the energy of the interaction between the inserted test molecule and the rest of the system,  $k_{\text{B}}$  is the Boltzmann

**TABLE 2: References and Geometry Parameters of the Potential Models Used for the Studied Solute Molecules**

molecule	ref	bond	bond length (Å)	angle	bond angle (deg)
H <sub>2</sub> O	27 <sup>a</sup>	O–H	0.975	H–O–H	104.5
O <sub>2</sub>	26 <sup>b</sup>	O–O	1.208		
CO	26 <sup>b</sup>	C–O	1.128		
CO <sub>2</sub>	31	C–O	1.230	O–C–O	180.0
NO	32	N–O	1.150		
NH <sub>3</sub>	33	N–H	1.012	H–N–H	106.7
CHCl <sub>3</sub>	34 <sup>c</sup>	CH–Cl	1.758	Cl–CH–Cl	111.3
formamide <sup>d</sup>	35 <sup>c</sup>	CH–O	1.229	O–CH–N	122.9
		CH–N	1.335	H–N–H	120.4
		N–H	0.960		

<sup>a</sup> TIP3P model. <sup>b</sup> CHARMM model. <sup>c</sup> OPLS model. <sup>d</sup> Molecule of planar geometry.

**TABLE 3: Interaction Parameters of the Potential Models Used for the Studied Solute Molecules**

molecule	atom	$\sigma/\text{\AA}$	$(\epsilon/k_{\text{B}})/\text{K}$	$q/e$
H <sub>2</sub> O	H			+0.417
	O	3.151	76.5	-0.834
O <sub>2</sub>	O	3.029	60.4	0.000
	C	3.742	55.4	+0.021
CO	O	3.029	60.4	-0.021
	C	3.262	61.9	+0.663
CO <sub>2</sub>	O	3.014	97.7	-0.3315
	C	3.262	61.9	+0.663
NO	N	3.250	85.6	+0.028
	O	3.120	80.1	-0.028
NH <sub>3</sub>	N	3.385	170.0	-1.035
	H			+0.345
CHCl <sub>3</sub>	CH	3.800	40.3	+0.420
	Cl	3.470	201.4	-0.140
formamide	O	2.960	105.7	-0.500
	CH	3.800	57.9	+0.500
	N	3.250	85.6	-0.850
	H			+0.425

factor, and  $T$  is the temperature.<sup>21</sup> The cavity insertion Widom variant<sup>22</sup> modifies the original algorithm by searching for cavities of the minimum radius of  $R_{\text{cav}}$  in the system and making insertions of the test molecule solely into such cavities. It should be noted that throughout this paper the term “cavity” means a spherical void in the system that does not contain the center of any atoms. The excess free energy  $A'$  of the inserted molecule can be obtained by the formula

$$A' = -k_{\text{B}}T[\ln\langle\exp(-U_{\text{test}}/k_{\text{B}}T)\rangle + \ln\langle P_{\text{cav}} \rangle - 1] - pV/N \quad (1)$$

where  $\langle \dots \rangle$  denotes ensemble averaging, and  $P_{\text{cav}}$  is the probability of finding a cavity with a radius of at least  $R_{\text{cav}}$ . The value of  $P_{\text{cav}}$  can be obtained from the calculation in a rather straightforward way, as the ratio of the number of cavities found and number of points checked in the cavity searching procedure.

**Free Energy Profile Calculations.** The free energy profile of eight solutes, i.e., H<sub>2</sub>O, O<sub>2</sub>, CO, CO<sub>2</sub>, NO, NH<sub>3</sub>, CHCl<sub>3</sub>, and formamide, has been calculated across the four simulated DMPC/cholesterol membrane systems by the CIW method. The solute molecules have been represented by rigid potential models interacting through Lennard-Jones and Coulombic interactions. The CH groups of the chloroform and formamide molecules have been represented as united atoms. The original references where the used potential models have been described as well as their geometrical parameters are summarized in Table 2, whereas the  $\sigma$  and  $\epsilon$  Lennard-Jones and  $q$  Coulombic interaction parameters are collected in Table 3 for all interaction sites of the models.

The free energy profiles have been calculated using the program MMC.<sup>25</sup> In the calculations, the systems have been

divided into 25 slabs along the bilayer normal axis denoted as  $z$  (being  $z = 0$  in the middle of the membrane), and the free energy values have been determined in each slab independently. Thus, following eq 1, the excess Helmholtz free energy profiles along the  $z$ -axis have been calculated as

$$A'(z) = -k_B T [\ln \langle \exp(-U_{\text{test}}(z)/k_B T) \rangle + \ln \langle P_{\text{cav}}(z) \rangle - 1] \quad (2)$$

The  $-pV/N$  term of eq 1 has been omitted in the calculation since at atmospheric pressure it gives only a negligibly small and  $z$ -independent contribution to the free energy. Cavities have been searched along grids in the simulation cell in such a way that each slab of the system along the  $z$ -axis has contained 7500 grid points. In each sample configuration, four of such grids have been set up, each differing from the other by a small shift, and thus, 30 000 points per slab have been checked in each configuration. The free energy profiles of all the eight solutes have been calculated with two different  $R_{\text{cav}}$  values, i.e., 2.6 and 2.8 Å. Test molecules have been inserted into each cavity found in 10 different, randomly selected orientations. Since it is sensible to assume that for the largest solutes only the largest cavities present in the system can give a considerable contribution to the energy average in eq 2, and because the omitting of the smaller cavities from the calculation speeds up the calculation allowing a better mapping of the system within the same computation time, we have repeated the FEP calculation of CO<sub>2</sub>, CHCl<sub>3</sub>, and formamide in all the four systems with the  $R_{\text{cav}}$  value of 2.9 Å, using 10 different random grids (i.e., 75 000 grid points per slab) in each configuration. Finally, for further reducing the noise of the results the obtained FEPs have been averaged over the two sides of the bilayers.

## Results and Discussion

**Estimation of the Precision of the Calculations.** In order to estimate the precision of the results obtained in the free energy profile calculations, we have calculated the excess solvation Helmholtz free energy of each of the eight solute molecules in pure water by the CIW and the original Widom method as well as by using the thermodynamic integration (TI) methodology<sup>36</sup> over a polynomial path,<sup>37</sup> and have compared the values obtained with these different methods. This TI methodology is fast and reliable for homogeneous systems, which makes it a suitable reference method for the present purpose. It should be noted, however, that the use of the TI methodology becomes much less advantageous when studying inhomogeneous systems, in particular, systems showing large local inhomogeneities (e.g., due to the slow conformational changes of the molecules), such as the hydrated DMPC/cholesterol mixed bilayers investigated here. In a previous study, we have demonstrated for CHCl<sub>3</sub> that the determination of its solvation free energy profile across a hydrated pure DMPC bilayer requires at least an order of magnitude longer computation when using the TI instead of a Widom-type methodology.<sup>22</sup>

The CIW and TI calculations of the excess solvation free energy of H<sub>2</sub>O, O<sub>2</sub>, CO, CO<sub>2</sub>, NO, and CHCl<sub>3</sub> in water have been published in our previous paper.<sup>22</sup> The calculations for NH<sub>3</sub> and formamide have been done in a similar way. Thus, the original Widom and the CIW calculations have been performed using 40 000 equilibrium sample configurations of 107 TIP3P water molecules at 310 K. Details of the water simulation are given elsewhere.<sup>22</sup> In the CIW calculations, cavities of radius at least  $R_{\text{cav}}$  have been searched along a 60 × 60 × 60 grid in each configuration. Two different  $R_{\text{cav}}$  values have been used, i.e., 2.6 and 2.8 Å. In the calculations using

**TABLE 4: Excess Hydration Free Energy of the Eight Solutes Studied at 310 K<sup>a</sup>**

solute	TI	original Widom	CIW, using $R_{\text{cav}} = 2.6 \text{ \AA}$	CIW, using $R_{\text{cav}} = 2.8 \text{ \AA}$
H <sub>2</sub> O <sup>b</sup>	$-5.74^c \pm 0.66$	-5.56	-5.39	-4.67
O <sub>2</sub> <sup>b</sup>	$2.81 \pm 0.74$	3.39	3.27	3.27
CO <sup>b</sup>	$3.29 \pm 0.83$	4.13	3.94	4.00
CO <sub>2</sub> <sup>b</sup>	$-0.03 \pm 0.77$	1.38	1.03	1.09
NO <sup>b</sup>	$2.29 \pm 0.70$	3.03	2.88	2.89
NH <sub>3</sub>	$-3.22 \pm 0.68$	-1.76	-2.00	-1.50
CHCl <sub>3</sub> <sup>b</sup>	$1.31 \pm 1.21$	3.77	3.64	2.91
formamide	$-8.11 \pm 0.94$	-5.43	-7.49	-6.25

<sup>a</sup> Values are in kcal/mol. <sup>b</sup> Ref 22. <sup>c</sup> Grand canonical Monte Carlo simulation resulted in the value of -5.75 kcal/mol, see ref 22.

the original Widom method, the test molecules have been inserted into positions defined by a 15 × 15 × 15 grid. In this way, the computational cost of the CIW calculations with the  $R_{\text{cav}}$  values of 2.6 and 2.8 Å have been about 10% and 75% less, respectively, than that of the original Widom-type calculations. In each case, the test molecule has been inserted in 10 different, randomly chosen orientations. The excess solvation free energy has been calculated using eq 1, being  $P_{\text{cav}} = 1.0$  in the case of the original Widom method.

In the TI calculations, we have parametrized the water–solute contribution to the total energy of the system  $U_{\text{w-s}}$  as

$$U_{\text{w-s}}(\lambda) = \lambda^4 U_{12} + \lambda^3 U_6 + \lambda^2 U_1 \quad (3)$$

where  $\lambda$  is the coupling parameter and  $U_i$  is the energy contribution of  $U_{\text{w-s}}$  depending on the site–site separation  $r$  as  $r^{-i}$  (i.e.,  $U_{12}$ ,  $U_6$ , and  $U_1$  are the Lennard-Jones repulsion, Lennard-Jones attraction, and Coulomb interaction terms of  $U_{\text{w-s}}$ , respectively). This path was shown to yield an integrand that is smooth and close to linear, allowing a precise estimate of the integral over the entire  $\lambda$  range of  $0 \leq \lambda \leq 1$  using only a few quadrature points.<sup>37,38</sup> The exponent 4 applied to the  $\lambda$  scaling of  $U_{12}$  is dictated by the fact that in three dimensions the  $r^{-12}$  repulsion term would make the integrand singular at  $\lambda = 0$ .<sup>36</sup> As is evident from eq 3, the reference (i.e.,  $\lambda = 0$ ) state of this path is the ideal gas state of the solute. The excess hydration free energy can then be obtained as

$$A' = \int_0^1 \left\langle \frac{\partial U_{\text{w-s}}(\lambda)}{\partial \lambda} \right\rangle_\lambda d\lambda = \int_0^1 (4\lambda^3 \langle U_{12} \rangle_\lambda + 3\lambda^2 \langle U_6 \rangle_\lambda + 2\lambda \langle U_1 \rangle_\lambda) d\lambda \quad (4)$$

Here the symbol  $\langle \dots \rangle_\lambda$  denotes ensemble averaging using  $U_{\text{w-s}}(\lambda)$  instead of the contribution of the water–solute interaction to the total energy in the Boltzmann factor. The integral has been evaluated numerically, using a 5-point Gaussian quadrature. The integrand has been calculated by performing a Monte Carlo simulation in each quadrature point. These simulations have been performed in the same way as the one for the CIW and Widom calculations.

The excess free energy values obtained by the different methods are summarized in Table 4. As is seen, the precision of the CIW method is about the same for NH<sub>3</sub> and formamide as for the other six solutes tested previously. Apart from the largest molecule, i.e., CHCl<sub>3</sub>, the CIW calculations are within about 0.3–1.2 kcal/mol (i.e., about 0.5–2  $k_B T$ ) of the reference values obtained by TI when the  $R_{\text{cav}}$  value of 2.6 Å is used. Moreover, the deviation of these CIW results from the reference TI data is usually smaller than the estimated error of the TI results themselves. The  $R_{\text{cav}}$  value of 2.8 Å leads to somewhat

less accurate results for most of the studied molecules but becomes the better choice for  $\text{CHCl}_3$ , when only positions located in the largest cavities are corresponding to low enough energy values and contribute noticeably to the average in eq 2. Nevertheless, the CIW result obtained with  $R_{\text{cav}} = 2.8 \text{ \AA}$  for  $\text{CHCl}_3$  still differs by 1.60 kcal/mol from the TI value, indicating that considerably smaller precision can be obtained for  $\text{CHCl}_3$  than for the other seven solutes by the CIW method. It is also evident that the CIW calculations with both choices of  $R_{\text{cav}}$  have led consistently to a somewhat better reproduction of the reference TI values than calculations performed with the original Widom method, even if calculations of the latter type have required considerably more computing time. As a general trend, the CIW method is found to work more precisely for smaller and less polar molecules.

It is clear from Table 4 that the excess free energy results obtained with the Widom method are generally higher than the reference TI values, and the use of larger limiting radii leads to higher solvation free energies. The reason for this is that, due to the averaging of the  $\exp(-U_{\text{test}}/k_{\text{B}}T)$  terms in the calculation (see eqs 1 and 2), the loss of low enough energy test insertions, which is unavoidable in a Widom-type sampling procedure, leads systematically to  $A'$  values that are too high. Moreover, the deviations of the results of the Widom-type calculations from the reference TI data are generally larger for larger solutes. This can be understood by realizing that with the increase of the solute size the probability of forming a large enough cavity becomes progressively smaller, and once the solute size exceeds significantly the size of the solvent, this probability is likely to be small enough that no such cavity is found during the simulation. This means that the most negative contributions are systematically excluded from the estimate of the free energy. This observation could also form the basis of an appropriate correction, but it has not been attempted in the present work.

The obtained differences between the CIW and TI results in pure water can be considered as an estimate for the limit of accuracy of the FEP calculations across the DMPC/cholesterol mixed bilayers, as it is quite sensible to assume that the method works with the same precision in the aqueous region of the membranes as in pure water. Moreover, better precision can be expected in the less dense and apolar region of the hydrocarbon chains. However, in the dense interfacial region, the CIW calculations can work with a smaller precision, in particular for larger solutes. These points should be kept in mind in the analysis of the FEPs across the membranes, and only such features of the resulting profiles should be interpreted which correspond to a considerably larger free energy difference than the estimated precision of the method.

**Cavity Profiles in the DMPC/Cholesterol Bilayers.** The  $P_{\text{cav}}(z)$  probability profiles of finding spherical cavities larger than a given minimum size along the bilayer normal axis  $z$  are shown in Figure 1 as obtained in the four systems simulated for three different values of the minimum cavity radius  $R_{\text{cav}}$ , i.e., 2.6, 2.8, and 2.9  $\text{\AA}$ . As is seen, the shape of the obtained profiles is rather similar for the different  $R_{\text{cav}}$  values in all the four systems. The profiles are roughly constant beyond about  $\pm 15 \text{ \AA}$ , in the aqueous and interfacial regions of the membranes, and increase steadily toward the middle of the bilayer in the hydrocarbon phase. It is also seen that the presence of cholesterol has rather little influence on the  $P_{\text{cav}}(z)$  profiles. The only region where cholesterol noticeably influences the amount of cavities present is between about  $\pm 10$  and  $20 \text{ \AA}$ , i.e., where the cholesterol OH groups are located.<sup>29</sup> As is seen, cavities are found with higher probabilities here in systems of higher

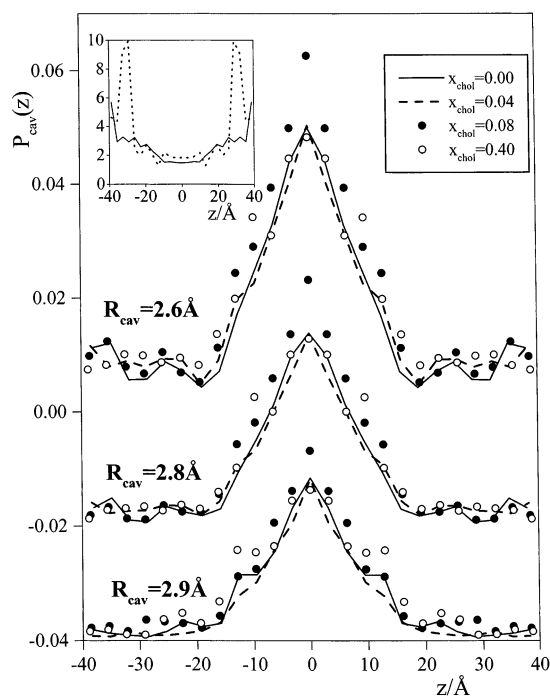


**Figure 1.** Probability profiles of finding spherical cavities of different minimum radii  $R_{\text{cav}}$  across the simulated fully hydrated DMPC/cholesterol mixed membranes: solid lines (—), system I; dashed lines (—), system II; full circles (●), system III; open circles (○), system IV. The results with  $R_{\text{cav}} = 2.8 \text{ \AA}$  and  $R_{\text{cav}} = 2.9 \text{ \AA}$  are shifted by  $-0.02$  and  $-0.04$ , respectively. The inset shows the ratio of the profiles with  $R_{\text{cav}} = 2.6 \text{ \AA}$  and  $R_{\text{cav}} = 2.8 \text{ \AA}$  (—), and with  $R_{\text{cav}} = 2.6 \text{ \AA}$  and  $R_{\text{cav}} = 2.9 \text{ \AA}$  (···) in system IV.

cholesterol concentration, and this effect is more expressed for smaller limiting cavity radius values. Thus, for the  $R_{\text{cav}}$  values of 2.6 and 2.8  $\text{\AA}$ , the  $P_{\text{cav}}(z)$  profile of system II is only slightly larger in this region than that of system I of pure DMPC, whereas systems III and IV of higher cholesterol content have  $P_{\text{cav}}$  values even larger than that for system II here. Also, in these systems the region in which  $P_{\text{cav}}(z)$  is higher than in pure DMPC is extended toward the middle of the bilayer. It is also seen that the  $P_{\text{cav}}(z)$  profiles of systems III and IV do not differ considerably even in this region, indicating that above a certain concentration this effect of cholesterol on the amount of cavities present is vanishing. On the other hand, for  $R_{\text{cav}} = 2.9 \text{ \AA}$ , only system IV, containing 40% cholesterol, has considerably higher  $P_{\text{cav}}$  values here than system I of pure DMPC, whereas the  $P_{\text{cav}}(z)$  profile of system II is even lower here than that of system I.

Contrary to the interfacial region, the  $P_{\text{cav}}(z)$  profiles seem to be independent from the concentration of cholesterol beyond  $\pm 20 \text{ \AA}$ , in the aqueous phase, and within  $\pm 8 \text{ \AA}$ , in the hydrocarbon region of the membrane. The only exception is that system III contains considerably more cavities in the middle of the bilayer than the other three systems. This independence of  $P_{\text{cav}}(z)$  from the amount of cholesterol present in the membrane seems to be rather obvious in the aqueous region. However, the observed behavior of  $P_{\text{cav}}(z)$  is rather interesting in the hydrocarbon phase, since the density profile of the membrane in this region has been found to be independent from the concentration of cholesterol only in the cholesterol-poor side of the DMPC/cholesterol miscibility gap, whereas in the cholesterol-rich side higher hydrocarbon phase densities have been observed.<sup>29</sup> This contrasts the present finding, indicating that (i) although the density of system III does not differ noticeably from that of systems I and II in the middle of the

membrane, it contains considerably more spherical cavities here than the other two systems, and (ii) although the density of system IV is considerably higher in the hydrocarbon region than that of systems I and II, the amount of spherical cavities is the same in these systems. These two points can be explained by assuming that cholesterol modifies the distribution of the free volume in the middle of the membrane: empty pockets are more spherical in the presence of cholesterol, whereas they are more elongated forming narrow channels in its absence. This is consistent with the finding of our previous study that the middle part of the hydrocarbon phase of the membrane becomes considerably more isotropic in the presence of a considerable amount of cholesterol than in its absence.<sup>29</sup> Such an effect of cholesterol on the distribution of free volume would (i) facilitate the solvation of relatively large molecules (i.e., that can only fit into the largest cavities present) in the hydrocarbon phase and (ii) make the diffusion of smaller or less spherical penetrants (i.e., that can even fit into the smaller cavities and pass through the empty channels) more difficult in membranes containing a considerable amount of cholesterol. Similar considerations can be made when comparing the density profiles<sup>29</sup> and  $P_{\text{cav}}(z)$  profiles of the systems in the aqueous and interfacial regions of the membranes. Namely, the density in the middle of the interfacial region, between  $\pm 15$ – $20$  Å, is about 20% higher than in the aqueous phase, beyond  $\pm 25$  Å, in all the four systems,<sup>29</sup> whereas the obtained  $P_{\text{cav}}(z)$  profiles are roughly constant beyond  $\pm 15$  Å. The fact that the concentration of spherical cavities is the same in the aqueous phase as in the dense interfacial region indicates that the free volume pockets are more spherical in the interfacial than in the aqueous region. These observations point out the importance of the distribution of size, shape, and connectivity of the free volume pockets along the bilayer normal in the determination of the permeability properties of the membrane. A detailed analysis of the free volume properties of the four membrane systems studied here, which is beyond the scope of the present paper, is currently in progress.

In order to investigate how the density of spherical cavities depends on their minimum size, we have also calculated the ratio of the  $P_{\text{cav}}(z)$  profiles resulting from different  $R_{\text{cav}}$  values. The inset of Figure 1 shows the ratio of the  $P_{\text{cav}}(z)$  profiles with  $R_{\text{cav}} = 2.6$  Å and  $R_{\text{cav}} = 2.8$  Å, and with  $R_{\text{cav}} = 2.6$  Å and  $R_{\text{cav}} = 2.9$  Å values in system IV. As is seen, in the dense interfacial as well as in the hydrocarbon region of the membrane, these ratios are around 2–3, indicating that the number of cavities with radii between 2.6 and 2.8–2.9 Å is about the same as with larger radii. On the other hand, in the aqueous phase these ratios increase up to 5–10, indicating that the density of cavities of radius larger than  $R_{\text{cav}}$  decreases sharply between the  $R_{\text{cav}}$  values of 2.6 and 2.8 Å in this region.

**Free Energy Profiles. Dependence of the Results on the Choice of Minimum Cavity Radius.** As is discussed in the previous section, the solvation free energy values determined by the CIW method should, in principle, depend on the arbitrary choice of the minimum cavity radius  $R_{\text{cav}}$ . Given that the same points are checked as possible cavity centers in the procedure and the same number of insertions are made in each cavity found, smaller  $R_{\text{cav}}$  values should lead to more precise results, as the increase of  $R_{\text{cav}}$  implies the neglect of several possible insertions. On the other hand, the use of larger  $R_{\text{cav}}$  values requires considerably less computing time, and hence in a calculation performed within the same time, more test points can be checked and more test insertions can be made, which can improve the precision of the results. In order to test how

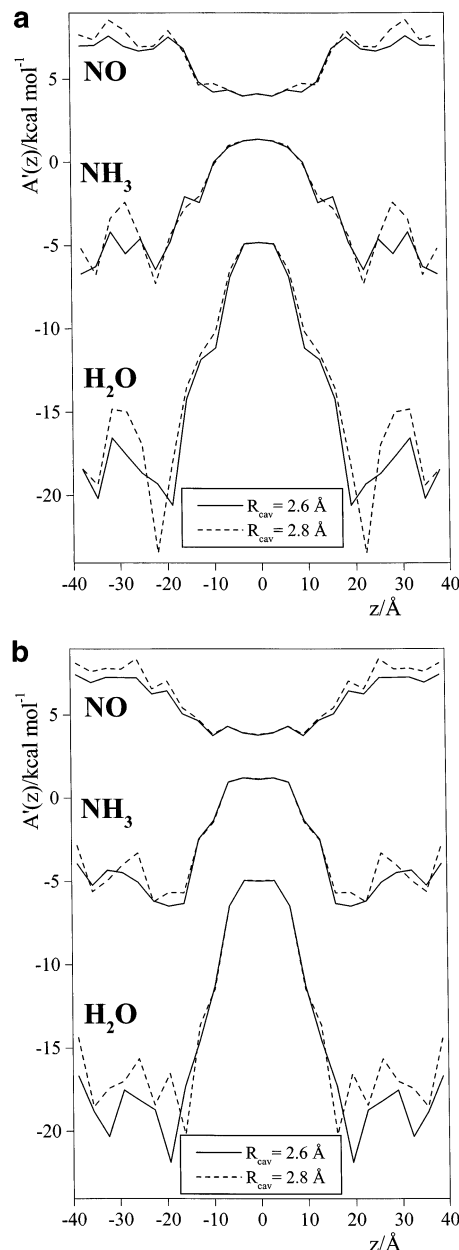


**Figure 2.** Free energy profiles of H<sub>2</sub>O, NH<sub>3</sub>, and NO as obtained by CIW calculation using the minimum cavity radius value of 2.6 Å (—) and 2.8 Å (—) in (a) system I (pure DMPC bilayer) and (b) system IV (bilayer containing 40% cholesterol). Results for H<sub>2</sub>O and NO are shifted by -7 and +3 kcal/mol, respectively.

the free energy profiles calculated are affected by the choice of  $R_{\text{cav}}$ , we have compared the free energy profiles obtained for three small penetrants, i.e., H<sub>2</sub>O, NH<sub>3</sub>, and NO, with the  $R_{\text{cav}}$  values of 2.6 and 2.8 Å (Figure 2), and for two larger penetrants (CO<sub>2</sub> and CHCl<sub>3</sub>) with the  $R_{\text{cav}}$  values of 2.6, 2.8, and 2.9 Å (Figure 3) in systems I and IV. It should be noted that while the calculations have been performed in the same way when using the  $R_{\text{cav}}$  values of 2.6 and 2.8 Å, in the case of  $R_{\text{cav}} = 2.9$  Å 2.5 times more grid points have been checked. As is seen from Figure 2, the choice of  $R_{\text{cav}} = 2.8$  Å has led, with only a few exceptions, to consistently higher solvation free energy values than the use of  $R_{\text{cav}} = 2.6$  Å in the interfacial and aqueous regions. This difference is due to the contribution of the test positions located in cavities of radius between 2.6 and 2.8 Å to the ensemble average of eq 2. However, the observed difference between the curves obtained with the two  $R_{\text{cav}}$  values is still rather small in all cases, being comparable with the precision

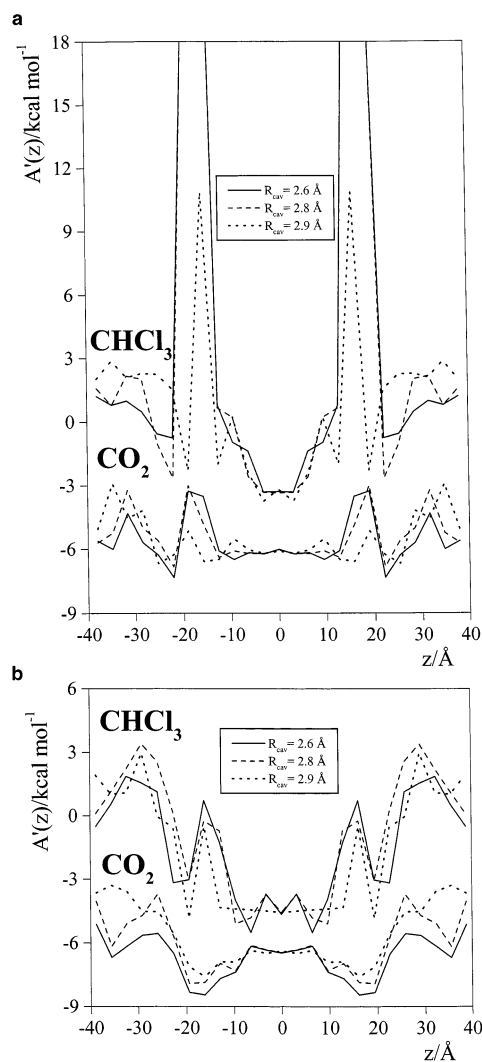


**Figure 3.** Free energy profiles of  $\text{CO}_2$  and  $\text{CHCl}_3$  as obtained by CIW calculation using the minimum cavity radius value of  $2.6 \text{ \AA}$  (—),  $2.8 \text{ \AA}$  (—), and  $2.9 \text{ \AA}$  (···) in (a) system I (pure DMPC bilayer) and (b) system IV (bilayer containing 40% cholesterol). Results for  $\text{CO}_2$  are shifted by  $-6 \text{ kcal/mol}$ .

of the method for these solutes as estimated in aqueous environment (see Table 4), and vanishes in the less dense hydrocarbon phase, where considerably more large cavities can be found than in the aqueous region (see Figure 1).

The comparison of the  $R_{\text{cav}} = 2.6 \text{ \AA}$  and  $R_{\text{cav}} = 2.8 \text{ \AA}$  free energy profiles leads to similar conclusions for the larger penetrants, although the difference of these curves is generally smaller here than for smaller solute molecules, as cavities of  $2.6 \text{ \AA} < R_{\text{cav}} < 2.8 \text{ \AA}$  are less likely to correspond to low enough energy for larger test molecules. The profiles obtained with  $R_{\text{cav}} = 2.9 \text{ \AA}$  behave similarly to those of  $R_{\text{cav}} = 2.8 \text{ \AA}$  for  $\text{CO}_2$ , indicating that the checking of more test points roughly compensates the neglect of cavities of radius between 2.8 and  $2.9 \text{ \AA}$  for this molecule. However, the situation is quite different for  $\text{CHCl}_3$ , where the choice of  $R_{\text{cav}} = 2.9 \text{ \AA}$  leads consistently to the lowest free energy values. Moreover, contrary to the case of smaller molecules for which the difference between the profiles obtained with different  $R_{\text{cav}}$  values remains within the estimated precision of the method, the choice of  $R_{\text{cav}}$  has a dramatic effect on the FEPR of chloroform in the dense interfacial region of system I, as seen in Figure 3a. This is due to the fact that for the large  $\text{CHCl}_3$  molecule only the largest cavities present in the systems can give considerable contribution

**TABLE 5: Dependence of the Average Excess Hydrational Free Energy on the Distance from the Lipid Bilayer**

system	no. water molecules	$Z (\text{\AA})$	$A'_{\text{H}_2\text{O}}$ (kcal/mol)	$A'_{\text{NH}_3}$ (kcal/mol)	$A'_{\text{NO}}$ (kcal/mol)
system I	2033	39.5	-12.81	-6.87	3.75
long box A	3045	50	-11.21	-7.02	4.29
long box B	3520	55	-10.59	-5.24	3.69
bulk water <sup>a</sup>	infinite		-5.39	-2.00	2.88
			(-5.00) <sup>b</sup>	(-2.76) <sup>b</sup>	(4.25) <sup>b</sup>

<sup>a</sup> See Table 4. <sup>b</sup> Values in parentheses are obtained by extrapolation from the linear fit of the  $A'(Z^{-1})$  data (see Figure 4).

to the energy average in eq 2, and hence, a more accurate search for such large cavities becomes far more important for a solute of this size than the inclusion of smaller cavities in the procedure.

Considering the results of these comparisons, the following analyses are performed with the choice of  $R_{\text{cav}} = 2.6 \text{ \AA}$  for all the penetrants, with the exception of  $\text{CHCl}_3$  for which the profiles obtained with the  $R_{\text{cav}}$  value of  $2.9 \text{ \AA}$  are used.

*Dependence of the Excess Hydrational Free Energy on the Distance from the Membrane.* As is seen from Figure 2, the excess hydrational free energy values obtained for  $\text{H}_2\text{O}$  in the aqueous phase of the membranes are falling in the range between  $-8$  and  $-13 \text{ kcal/mol}$ , considerably lower than the value of  $-5.39 \text{ kcal/mol}$  obtained in bulk water (see Table 4). A similar, although smaller, difference is found between the excess hydrational free energy of  $\text{NH}_3$  as calculated in bulk water and in the aqueous side of the bilayers. This effect of the vicinity of a lipid membrane on the excess hydrational free energy of polar solutes has already been observed in our previous study.<sup>22</sup> Unfortunately, the resulting free energy profiles are rather noisy, which makes it difficult to analyze in the aqueous phase their dependence on the distance from the bilayer. Nevertheless, it is quite clear that the hydrational free energy values of these solutes are increasing as they are getting farther apart from the membrane. It should be noted that similar behavior of  $A'_{\text{H}_2\text{O}}(z)$  has been observed in the vicinity of the water/1,2-dichloroethane liquid–liquid interface.<sup>39</sup>

In order to analyze the dependence of the excess hydrational free energy on the distance of the apolar phase, we have performed two more simulations of the pure DMPC bilayer. These simulations have been done in the same way as in the case of system I, with the only difference that the first of these systems (referred to as “long box A”) contained 3045, whereas the second system (“long box B”) contained 3520, water molecules, and the heights of the hexagonal prism shaped simulation cells have been increased accordingly. We have calculated the free energy profile of three solutes, i.e.,  $\text{H}_2\text{O}$ ,  $\text{NH}_3$ , and  $\text{NO}$ , in these long box systems in the same way as in system I with the  $R_{\text{cav}}$  value of  $2.6 \text{ \AA}$ . Since the resulting profiles are as noisy as in system I, we have averaged the excess hydrational free energy values over the  $z$  range of the width of 30% of the total box height, located farthest from the membrane. The distance of the middle of the slab considered from the middle of the membrane, denoted as  $Z$ , and the resulting average excess hydrational free energy values are summarized in Table 5 for all the three solutes. For comparisons, the table also contains the  $A'$  values obtained in pure water. The resulting  $A'$  values are plotted against  $Z^{-1}$  in Figure 4. As is seen, the resulting  $A'(Z^{-1})$  points can well be fitted by linear functions. The fitted lines are found to be steeper for more polar solutes (the dipole moment of the  $\text{H}_2\text{O}$ ,  $\text{NH}_3$ , and  $\text{NO}$  models used are  $2.391 \text{ D}$ ,  $1.894 \text{ D}$ , and  $0.155 \text{ D}$ , respectively). When fitting a straight line to the  $A'(Z^{-1})$  points obtained from the membrane

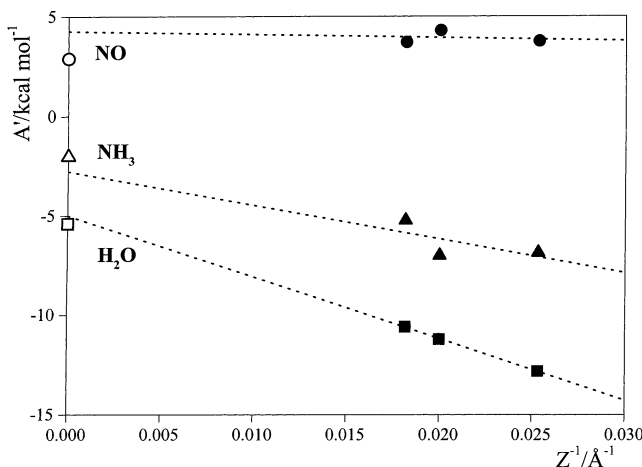


**Figure 4.** Dependence of the excess hydration free energy  $A'$  of  $\text{H}_2\text{O}$  (■, □),  $\text{NH}_3$  (▲, △) and  $\text{NO}$  (●, ○) on the reciprocal distance from a bilayer of DMPC  $Z^{-1}$ . Full symbols refer to values obtained from simulations of fully hydrated DMPC bilayers; empty symbols show values obtained in pure water. The straight lines fitted to the  $A'(Z^{-1})$  data obtained from the membrane simulations are also shown (—).

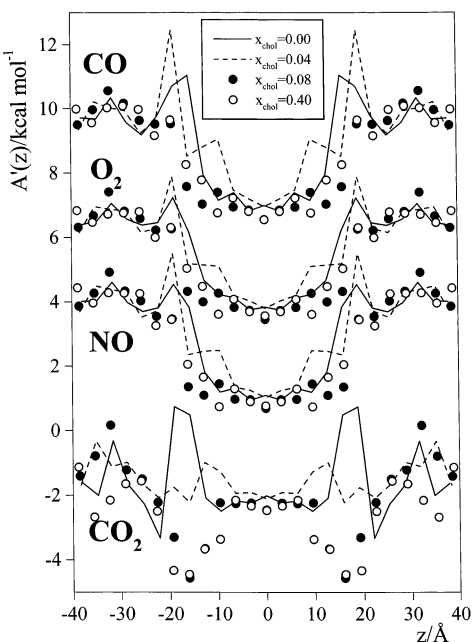


**Figure 5.** Free energy profiles of apolar or weakly polar solutes across the simulated fully hydrated DMPC/cholesterol mixed membranes. Solid lines (—), system I; dashed lines (—), system II; full circles (●), system III; open circles (○), system IV. The results for  $\text{CO}_2$ ,  $\text{O}_2$ , and  $\text{CO}$  are shifted by -2, +2, and +5 kcal/mol, respectively.

simulations, the excess free energy value corresponding to pure water (i.e., infinite distance from the membrane, at  $Z^{-1} = 0$ ) can be extrapolated. These extrapolated values, listed also in Table 5, agree well, within the precision of the CIW method, with the values obtained in bulk water for the two polar solutes. In the case of  $\text{NO}$ , this agreement is somewhat worse; however, for apolar or weakly polar solutes the difference between the excess hydration free energy values obtained in the aqueous phase of the membranes and in pure water is rather small, not considerably larger than the precision of the method itself.

**Discussion of the Obtained Free Energy Profiles.** The free energy profiles of the eight solute molecules studied across the four simulated DMPC/cholesterol mixed membranes are shown in Figures 5–7. As is seen, cholesterol has rather little influence on the excess solvation free energy of these molecules in the

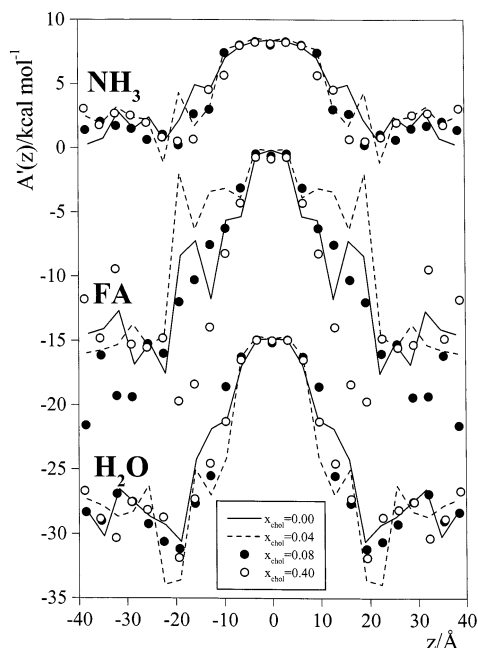


**Figure 6.** Free energy profiles of hydrogen bonding solutes across the simulated fully hydrated DMPC/cholesterol mixed membranes. Solid lines (—), system I; dashed lines (—), system II; full circles (●), system III; open circles (○), system IV. The results for  $\text{H}_2\text{O}$  and  $\text{NH}_3$  are shifted by -17 and +7 kcal/mol, respectively.

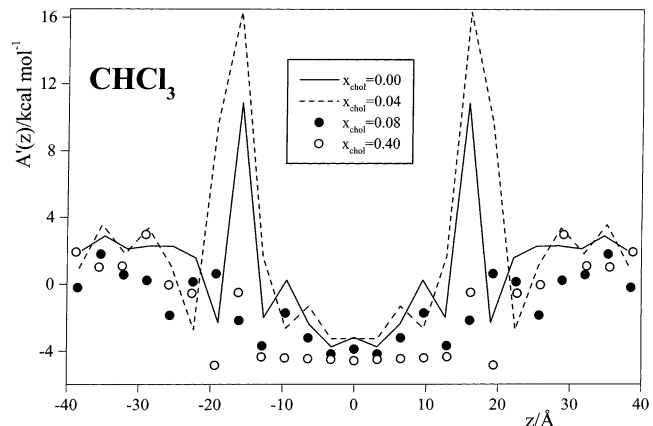


**Figure 7.** Free energy profiles of  $\text{CHCl}_3$  across the simulated fully hydrated DMPC/cholesterol mixed membranes. Solid line (—), system I; dashed line (—), system II; full circles (●), system III; open circles (○), system IV.

aqueous phase as well as in the middle of the bilayers. On the other hand, the presence of cholesterol in the membrane clearly decreases the free energy of all solutes in the  $|z|$  range between 10 and 20 Å, where the cholesterol OH groups are located,<sup>29</sup> indicating that it can considerably modify the thermodynamics of the crossmembrane transport of these penetrants. This finding is consistent with the previously discussed observation that the amount of spherical cavities is increased in this  $z$  range in the presence of cholesterol (see Figure 1). The present results indicate that the influence of cholesterol on the free energy profile, and thus on the permeability properties of small molecules, is closely related to its effect of modifying the distribution of the free volume in the membrane by replacing the phospholipid molecules by considerably shorter cholesterol. The  $|z|$  range around 20 Å is of particular importance in the free energy profile of many solutes. This is the outer boundary of the region of the cholesterol OH groups; i.e., the head of only the few cholesterol approaching closest to the interface

is located here, whereas most of the cholesterol molecules are not extended that far toward the outer membrane regions.<sup>29</sup>

It is also evident from Figures 5–7 that whereas the presence of cholesterol in the membrane has important consequences on the free energy profiles, its concentration has only a minor effect on them. The profiles obtained in system III, containing 8% cholesterol, do not differ considerably from those in system IV of 40% cholesterol content for most of the solutes. The reason for this is the fact that the excess solvation free energy of a molecule in a given environment is determined by those possible local arrangements in which its energy is the lowest, since a solvated molecule is almost exclusively located in local environments of minimum solvation energy. In the CIW calculation, this is realized by the fact that only the lowest energy test insertions give considerable contributions to the ensemble average in eqs 1 and 2. Hence, if a molecule can find lower energy positions in the vicinity of a cholesterol molecule than among the chains of the DMPC molecules, then adding cholesterol to a DMPC membrane lowers its solvation free energy by providing such possible low energy positions; however, the increase of the cholesterol concentration does not decrease further the solvation free energy considerably.

The calculated crossmembrane free energy profiles of the apolar or weakly polar solutes are plotted in Figure 5. As is seen, the profiles of the three diatomic molecules are rather similar to each other in the membranes of all four compositions. The excess solvation free energy profiles of these molecules are constant beyond  $\pm 20$  Å, in the aqueous and interfacial regions, and between  $\pm 20$  Å and  $\pm 10$  Å they decrease steadily toward the middle of the membrane, where they are constant again. The roughly 3.5 kcal/mol difference in the excess solvation free energy of these solutes in the aqueous phase and in the middle of the membranes represents the free energy barrier these penetrants have to go through when crossing these membranes. It is also seen that the  $|z|$  range where cholesterol lowers the solvation free energy, i.e., between 10 Å and 20 Å, coincides with the range in which the solvation free energy of these solutes changes monotonically from the aqueous phase value to the value characteristic of the middle of the membrane. Therefore, cholesterol does not alter the free energy barrier, and thus, the thermodynamic driving force of the crossmembrane transport of these molecules just makes the transition range of these profiles narrower.

The situation is somewhat different for  $\text{CO}_2$ . Here the difference between the free energy values characteristic of the aqueous and hydrocarbon phase is very small, about 1 kcal/mol, which is comparable with the estimated accuracy of the method (see Table 4). In the absence of cholesterol, there is a peak on the free energy profile between  $\pm 10$  and 20 Å. This peak is due to the fact that in the densest part of the bilayer<sup>29</sup> it is relatively difficult to accommodate a molecule as large as  $\text{CO}_2$ . However, this peak disappears in system II, containing 4% cholesterol, and becomes a dip in the systems of higher cholesterol content. Hence, adding cholesterol to a membrane of pure DMPC lowers the free energy barrier of the crossmembrane penetration of  $\text{CO}_2$  up to a certain concentration, whereas further increase of the cholesterol content results in an increase of this barrier again. Thus, a  $\text{CO}_2$  molecule has to go through two consecutive free energy barriers of about 2.5–3.5 kcal/mol when crossing either a membrane of pure DMPC or a mixed DMPC/cholesterol membrane of high enough cholesterol concentration. On the other hand, in mixed membranes of low enough cholesterol concentration a  $\text{CO}_2$  molecule can go through almost freely, the free energy barrier of such transport is found

to be comparable with the accuracy of the present calculation. It is well-known that  $\text{CO}_2$  can pass through real biological membranes much faster than either  $\text{CO}$  or  $\text{O}_2$ .<sup>2</sup> In light of the present study, this fact can be interpreted that, contrary to  $\text{CO}$  or  $\text{O}_2$ ,  $\text{CO}_2$  can permeate almost freely through the cholesterol-poor domains of the cell membranes.

Figure 6 shows the free energy profiles of the three strongly polar, hydrogen bonding solutes studied. The general shape of these profiles differs considerably from that of the diatomics as well as of  $\text{CO}_2$ . As discussed in detail in the previous subsection, the solvation free energy profiles of these molecules decrease steadily from the bulk phase of water toward the vicinity of the membrane. In the inner part of the interfacial region, at about  $z = \pm 20$  Å, these profiles go through a minimum, increase sharply upon further entering into the hydrocarbon phase, and go through a maximum in the middle of the membrane. The free energy difference between the minimum and maximum of the obtained profiles in pure DMPC has been found about 13, 6.5, and 13 kcal/mol for  $\text{H}_2\text{O}$ ,  $\text{NH}_3$ , and formamide, respectively. It should be noted that, despite the serious simplifications made in the present modeling of membranes of living cells, the obtained height of the free energy barrier of the crossmembrane penetration of a water molecule is in excellent agreement with experimental data obtained for two biological membranes, i.e., 13.6 and 12.9 kcal/mol.<sup>40</sup> The free energy lowering effect of cholesterol mostly affects that part of these profiles where they are increased from their minimum value in the interfacial region to their maximum in the middle of the membrane. However, the position of the minimum of these profiles around  $\pm 20$  Å is still in the  $z$  range where the presence of cholesterol can decrease the solvation free energy. Therefore, adding cholesterol to the membrane lowers also this minimum and, hence, increases the free energy difference between this minimum and the maximum in the hydrocarbon region, i.e., the free energy barrier these molecules have to go through when passing through the membrane. In this way, cholesterol can clearly decrease the permeability of the membrane for such strongly polar penetrants.

Finally, the obtained crossmembrane free energy profiles of  $\text{CHCl}_3$  in the four systems simulated are shown in Figure 7. The profiles obtained in systems I and II are markedly different from the profiles of all the other solutes investigated. The solvation free energy is found to be about 4 kcal/mol lower in the hydrocarbon region of the membrane than in the aqueous phase. However, the profiles go through a huge barrier in the dense interfacial region. This barrier is similar but much higher than what has also been found for  $\text{CO}_2$  in system I, due to the fact that the  $\text{CHCl}_3$  molecule is considerably larger than  $\text{CO}_2$ . Since it is rather difficult to find low enough energy positions for the test insertions of the large  $\text{CHCl}_3$  molecule in this dense region, the exact height of this barrier cannot be reliably estimated by a CIW calculation, and thus, the obtained profiles should only be interpreted in a qualitative way. Therefore, it can only be stated reliably on the basis of the present calculation that large free energy barriers exist in the dense region of DMPC membranes containing no cholesterol or of low cholesterol content for  $\text{CHCl}_3$ . However, when the cholesterol content of the membrane is increased up to 8%, this barrier completely disappears, and the resulting free energy profile becomes similar to those of the diatomic solutes. Further increase of the cholesterol concentration in the membrane does not change the free energy profile of  $\text{CHCl}_3$  considerably. It should be noted that the anaesthetic behavior of  $\text{CHCl}_3$  is related to the fact that  $\text{CHCl}_3$  can temporarily be dissolved in the interior of the cell

membrane and leave the membrane several orders of magnitude slower than any of the other solute molecules studied here. Although this behavior is consistent with the existence of a large free energy barrier for  $\text{CHCl}_3$  in membranes of low cholesterol content, it is not consistent with the lack of such a barrier in cholesterol-rich membranes. Thus, the present study points out that the anaesthetic behavior of  $\text{CHCl}_3$  cannot be explained simply by thermodynamic arguments, i.e., by the height of the free energy barrier of its crossmembrane transport, at least in the cholesterol-rich domains of the membrane, and hence, in these domains other reasons must be responsible for such behavior.

## Conclusions

The results of the present study clearly point out that the effect of cholesterol on the permeability properties of phospholipid membranes is, at least partly, originating in the fact that cholesterol modifies the free volume properties of the membrane in the hydrocarbon phase. Thus, in the region where the cholesterol OH groups are located, the density of spherical cavities of a given minimum radius is increased with increasing cholesterol concentration, and this effect is stronger for smaller limiting cavity radius values. This behavior is the consequence of two main reasons. First, at high cholesterol concentrations, the density of the membrane in this region is considerably smaller than at low cholesterol concentrations or in the absence of cholesterol,<sup>29</sup> and hence, there is more free volume available in cholesterol-rich than in cholesterol-poor or cholesterol-free membranes. However, at low cholesterol concentrations, this density decreasing effect of cholesterol is marginal.<sup>29</sup> In such membranes, the increase of the number of spherical cavities relative to the pure DMPC membrane results from the fact that the *distribution* of the free volume is changed by cholesterol: in the region of the cholesterol OH groups as well as in the middle of the membrane, free volume pockets are more spherical in the presence than in the absence of cholesterol.

The increased number of spherical cavities of a given minimum size in the region of the cholesterol OH groups, and, in particular, around the outer boundary of this region, results in lower solvation free energy values here for all penetrants investigated. This change, however, affects the free energy barrier of the crossmembrane transport of different penetrants in different ways, depending on the shape of their free energy profiles. Thus, for apolar or weakly polar diatomic solutes, the height of the free energy barrier is not affected by the presence of cholesterol, as the region where cholesterol lowers the solvation free energy corresponds to the monotonic transition part of the free energy profiles from their minimum in the middle of the membrane to the maximum in the aqueous phase. In the case of strongly polar, hydrogen bonding solutes, this effect of lowering the solvation free energy by cholesterol affects the region where the minimum of the free energy profiles is located. Hence, by lowering the minimum of their free energy profiles and leaving the maximum unchanged, cholesterol increases the free energy barrier of the crossmembrane transport of such penetrants, and hence reduces the permeability of the membrane for these molecules. The free energy profiles of apolar or moderately polar penetrants of larger size, such as  $\text{CO}_2$  and  $\text{CHCl}_3$ , exhibit a free energy peak in the dense region of pure DMPC membrane, where cholesterol can lower solvation free energy. For penetrants of larger size, such as  $\text{CHCl}_3$ , this peak is rather high, and hence, its lowering or elimination by cholesterol reduces the free energy barrier of the crossmembrane transport considerably. On the other hand, for  $\text{CO}_2$  this peak is

found to be only about 2–3 kcal/mol high, and it is transformed to a dip of about the same depth in the presence of sufficient amount of cholesterol. In this way, the free energy barrier of the crossmembrane transport remains unchanged. However, at small cholesterol concentrations, the transformation of this peak to a dip is not completed yet, and thus, at a certain concentration the intermediate stage of this transformation results in a flat free energy profile. This concentration is estimated to be about 4% in the present study. Thus, upon increasing the concentration of cholesterol from zero up to a certain, low concentration value, the permeability of the membrane for  $\text{CO}_2$  is found to increase, whereas further increase of the cholesterol concentration results in decreasing permeability.

Finally, it should be pointed out that the present analysis has only targeted the free energy profile of the studied penetrants, which is only one of the factors determining the permeability of the membrane. The other important factor in this respect is the diffusion profile of the penetrant molecules across the membrane (see the inhomogeneous solubility-diffusion model of Marrink and Berendsen),<sup>16,17</sup> which is not accessible by Monte Carlo simulations. However, our findings on the free volume distribution can provide some qualitative hints also in this respect. Thus, in the absence of cholesterol, free volume is distributed in a less spherical way in the hydrocarbon phase of the membrane than in its presence. Elongated voids can form narrow channels easier than spherical cavities, and thus facilitate the diffusion of small solutes of elongated shape, while making the diffusion of larger spherical penetrants more difficult. In order to clarify this point, a detailed analysis of the free volume properties, including the investigation of the size and shape distribution as well as connectivity properties of the free volume pockets across these membranes, would be of great importance. Work in this direction is currently in progress.

**Acknowledgment.** P.J. is a Magyary Zoltán fellow of the Foundation for Hungarian Research and Higher Education, Ministry of Education, Hungary, which is gratefully acknowledged. P.J. acknowledges support of the Hungarian OTKA Foundation under Project F038187, and of INTAS under Project 2001-0067. The authors also acknowledge access to the computer facilities at the Institute of Computational Biomedicine (ICB) of the Mount Sinai Medical Center.

## References and Notes

- (1) Hille, B. *Ionic Channels of Excitable Membranes*; Sinauer Associates: Sunderland, MA, 1992.
- (2) Guyton, A. C.; Hall, J. E. *Textbook of Medical Physiology*; W. B. Saunders: Philadelphia, 1996.
- (3) Finkelstein, A. *J. Gen. Physiol.* **1976**, *68*, 127.
- (4) Garthwaite, J.; Boulton, C. L. *Annu. Rev. Physiol.* **1995**, *57*, 683.
- (5) Sackmann, E. In *Structure and Dynamics of Membranes*; Lipowsky, R., Sackmann, E., Eds.; Elsevier: Amsterdam, 1995; pp 1–64.
- (6) Vist, M. R.; Davis, J. H. *Biochemistry* **1990**, *29*, 451.
- (7) McMullen, T. P. W.; McElhaney, R. N. *Biochim. Biophys. Acta* **1995**, *1234*, 90.
- (8) Radhakrishnan, A.; McConnell, H. M. *J. Am. Chem. Soc.* **1999**, *121*, 486.
- (9) Radhakrishnan, A.; McConnell, H. M. *Biophys. J.* **1999**, *77*, 1507.
- (10) Keller, S. L.; McConnell, H. M. *Phys. Rev. Lett.* **1999**, *82*, 1602.
- (11) Richter, F.; Finegold, L.; Rapp, G. *Phys. Rev. E* **1999**, *59*, 3483.
- (12) Carruthers, A.; Melchior, D. L. *Biochemistry* **1983**, *22*, 5797.
- (13) Bittman, R.; Clejan, S.; Lund-Katz, S.; Phillips, M. C. *Biochim. Biophys. Acta* **1984**, *772*, 117.
- (14) Subczynski, W. K.; Wisniewska, A.; Yin, J.-J.; Hyde, J. S.; Kusumi, A. *Biochemistry* **1994**, *33*, 7670.
- (15) Xiang, T.-X.; Anderson, B. D. *Biophys. J.* **1997**, *72*, 223.
- (16) Marrink, S. J.; Berendsen, H. J. C. *J. Phys. Chem.* **1994**, *98*, 4155.
- (17) Marrink, S. J.; Berendsen, H. J. C. *J. Phys. Chem.* **1996**, *100*, 16729.

(18) Jedlovszky, P.; Mezei, M. Unpublished results.

(19) Bassolino-Klimas, D.; Alper, H. E.; Stouch, T. R. *J. Am. Chem. Soc.* **1995**, *117*, 4118.

(20) Stouch, T. R.; Bassolino, D. In *Biological Membranes*; Merz, K. M., Roux, B., Eds.; Birkhäuser: Boston, 1996; pp 255–280.

(21) Widom, B. *J. Chem. Phys.* **1963**, *39*, 2808.

(22) Jedlovszky, P.; Mezei, M. *J. Am. Chem. Soc.* **2000**, *122*, 5125.

(23) Mezei, M. *Mol. Phys.* **1980**, *40*, 901.

(24) Mezei, M. *Mol. Phys.* **1987**, *61*, 565; **1989**, *67*, 1207 (erratum).

(25) URL: <http://inka.mssm.edu/~mezei/mmc>.

(26) Schlenkirch, M.; Brickmann, J.; MacKerell, A. D., Jr.; Karplus, M. In *Biological Membranes*; Merz, K. M., Roux, B., Eds.; Birkhäuser: Boston, 1996; pp 31–82.

(27) Jorgensen, W. L.; Chandrashekhar, J.; Madura, J. D.; Impey, R.; Klein, M. L. *J. Chem. Phys.* **1983**, *79*, 926.

(28) Alper, H. E.; Bassolino, D.; Stouch, T. R. *J. Chem. Phys.* **1993**, *98*, 9798.

(29) Jedlovszky, P.; Mezei, M. *J. Phys. Chem. B.*, *107* 5311.

(30) Jedlovszky, P.; Mezei, M. *J. Chem. Phys.* **1999**, *111*, 10770.

(31) Somasundaram, T.; in het Panhuis, M.; Lynden-Bell, R. M.; Patterson, C. H. *J. Chem. Phys.* **1999**, *111*, 2190.

(32) Li, H.; Elber, R.; Straub, J. E. *J. Biol. Chem.* **1983**, *268*, 17908.

(33) Kristóf, T.; Vorholz, J.; Liszsi, J.; Rumpf, B.; Maurer, G. *Mol. Phys.* **1999**, *97*, 1129.

(34) Jorgensen, W. L.; Briggs, J. M.; Contreras, M. L. *J. Phys. Chem.* **1990**, *94*, 1683.

(35) Jorgensen, W. L.; Swenson, C. J. *J. Am. Chem. Soc.* **1985**, *107*, 569.

(36) Mezei, M.; Beveridge, D. L. *Ann. N.Y. Acad. Sci.* **1986**, *482*, 1.

(37) Mezei, M. *J. Comput. Chem.* **1992**, *13*, 651.

(38) Resat, H.; Mezei, M. *J. Chem. Phys.* **1993**, *99*, 6052.

(39) Jedlovszky, P.; Vincze, Á.; Horvai, G. *J. Mol. Liq.*, in press.

(40) Jansson, T.; Illsley, N. P. *J. Membr. Biol.* **1993**, *132*, 147.